Supplementary Information

Reforming material chemistry of CIGS solar cells via a precise Ag doping strategy

Jiseon Hwang,[a,b] Ha Kyung Park,[c] Donghyeop Shin,[a] Inyoung Jung,[a] Inchan Hwang,[a] Young-Joo Eo,[a] Ara Cho,[a] Joo Hyung Park,[a] Soomin Song,[a] Yunae Cho,[a,c] Jihye Gwak,[d,e] Hyo Sik Jang,*[b] William Jo*[c] and Kihwan Kim*[a,e]

[a] Photovoltaics Research Department, Korea Institute of Energy Research, Daejeon 34129, Republic of Korea

[b] Graduate School of Energy Science and Technology (GEST), Chungnam National University, Daejeon 34134, Republic of Korea

[c] Department of Physics, Ewha Womans University, Seoul 03760, Republic of Korea

[d] New and Renewable Energy Institute, Korea Institute of Energy Research, Daejeon 34129, Republic of Korea

[e] University of Science and Technology, Daejeon 34113, Republic of Korea

* Corresponding authors: hschang@cnu.ac.kr, wmjo@ewha.ac.kr and kimkh@kier.re.kr

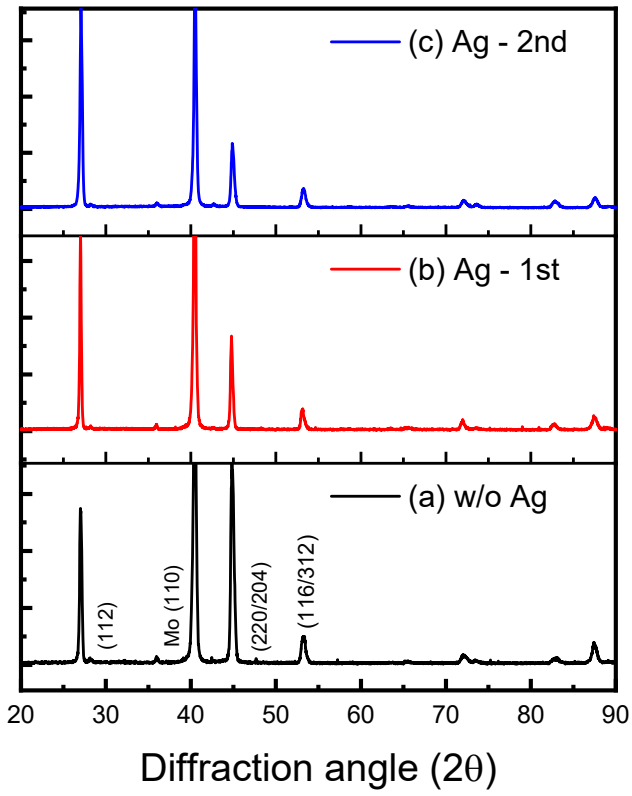

Fig. S1 XRD (θ-2θ scan) patterns of CIGS and ACIGS films. The Ag incorporation was found to weaken (220)/(204) preferred orientation. The ACIGS films showed (112) preferred orientation similar to the powder pattern of chalcopyrite.

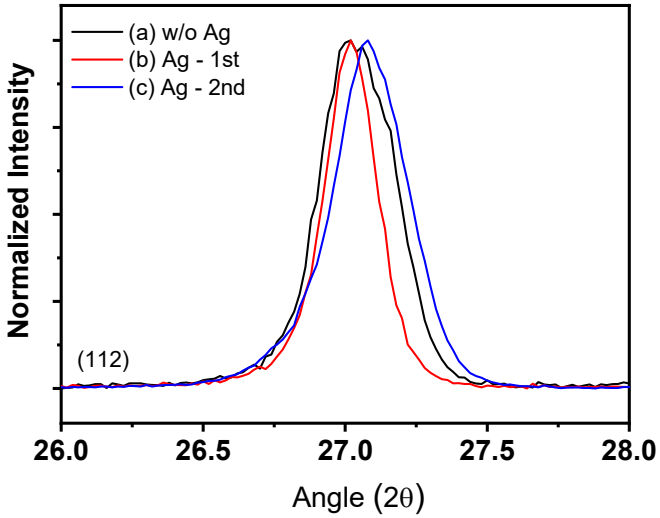

Fig. S2 (112) XRD (θ-2θ scan) patterns of CIGS films. The CIGS film (i.e., control) shows broad (112) reflections that originate from relatively inhomogeneous Ga/(Ga+In) compositional depth profiles and the ACIGS film (Ag incorporation in the second stage) appeared to exhibit a slightly higher Ga/(Ga+In) ratio than the others, which is verified by the SIMS analyses.

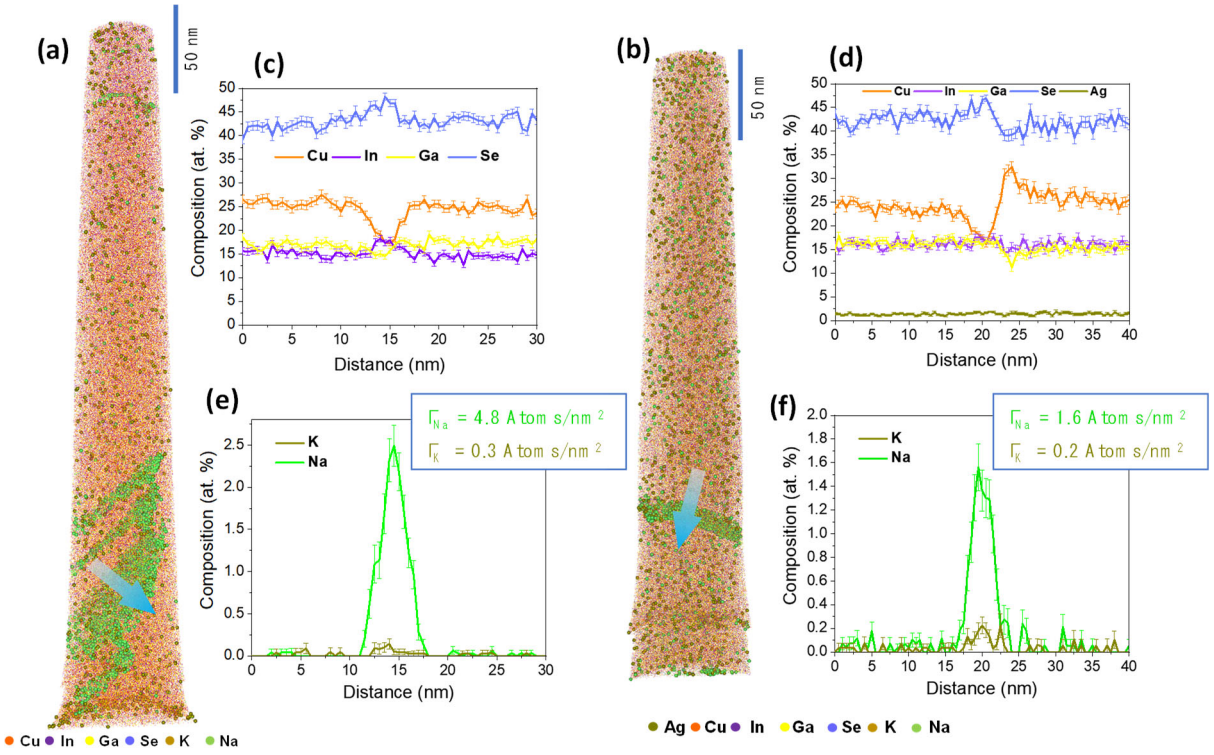

Fig. S3 Further APT results of CIGS without and with Ag incorporation: 3D atom maps of (a) CIGS and (b) ACIGS specimens; 1D concentration profiles of matrix elements: (c) without and (d) with Ag incorporation; and 1D concentration profiles of alkali (Na and K) elements: (e) without and (f) with Ag incorporation.

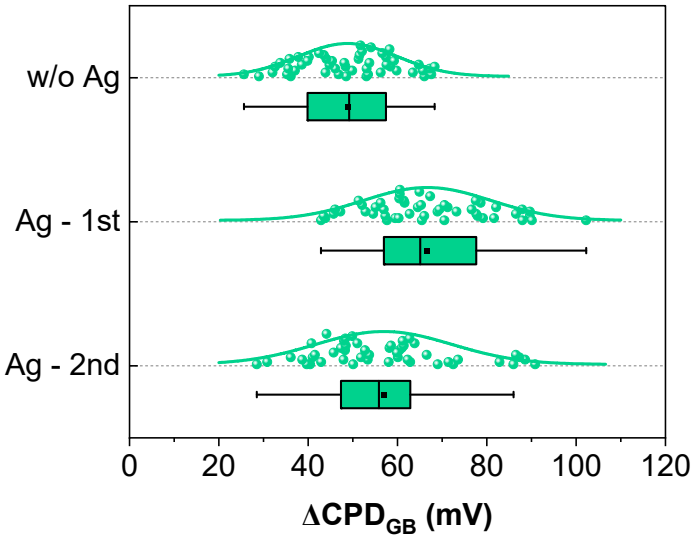

Fig. S4 Box plot of the extracted ΔCPD_{GB} values (ΔCPD_{GB}= CPD_{GB}-CPD_{IG}). The CIGS sample with Ag incorporation in the first stage showed the highest average of ΔCPD_{GB} and that of the CIGS sample without Ag was the lowest. The CIGS sample with Ag incorporation in the second stage showed a relatively wide range of ΔCPD_{GB} values indicating inhomogeneous CPD value distribution.

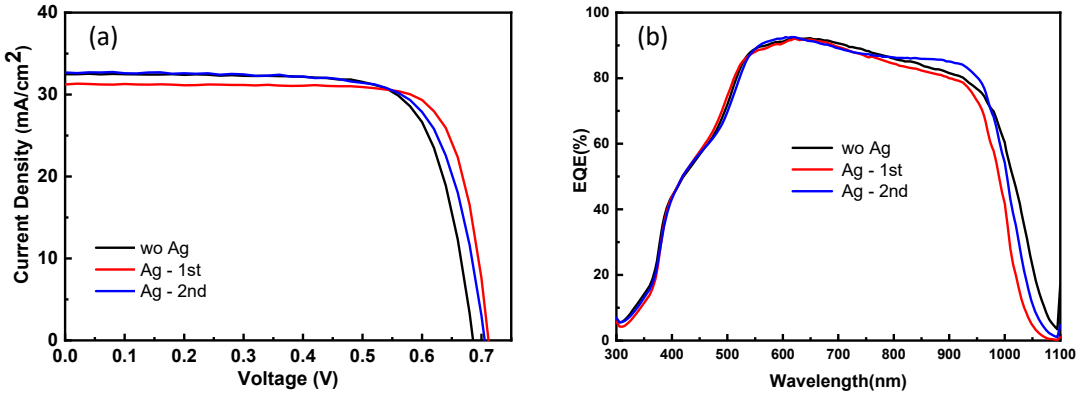

Fig. S5 Illuminated JV (a) and external quantum efficiency (EQE) (b) curves of the best CIGS solar cells in each case.

Table S1. Illuminated JV characteristics of CIGS solar cells of Fig. S5.

	Eff (%)	FF (%)	V_{OC} (V)	J_{SC} (mA/cm^2)
(a) wo Ag	16.7	75.1	0.686	32.5
(b) Ag – 1st	17.6	79.2	0.712	31.2
(c) Ag – 2nd	17.0	73.8	0.705	32.7

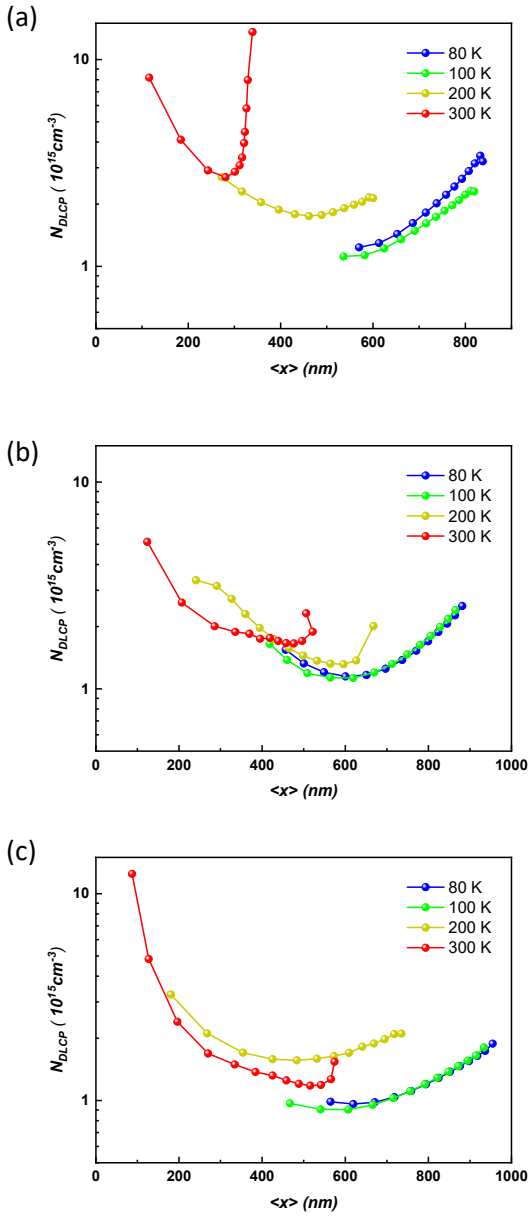

Fig. S6 Drive-level capacitance profiling (DLCP) curves of CIGS solar cells: (a) control, (b) Ag incorporation in the first stage, and (c) Ag incorporation in the second stage.

Table S2. Moment of charge response (<x>) and drive-level density (N_{DLCP}) values derived from Fig. S6.

	Temperature	<x> nm	N_{DLCP} (10^{15}/cm^3)
Without Ag (control)	80 K	714.40	1.82
	100 K	690.40	1.49
	200 K	431.01	1.79
	300 K	301.12	2.87
Ag - first stage	80 K	651.06	1.17
	100 K	619.27	1.13
	200 K	394.02	1.98
	300 K	369.66	1.85
Ag - second stage	80 K	758.85	1.11
	100 K	715.24	1.02
	200 K	483.38	1.56
	300 K	334.22	1.49